Available online at www.sciencedirect.com
ScienceDirect
Journal of Solid State Chemistry 179 (2006) 3330–3337
JOURNAL OF SOLID STATE CHEMISTRY
www.elsevier.com/locate/jssc

A study of the reactivity of elemental Cr/Se/Te thin multilayers using X-ray reflectometry, in situ X-ray diffraction and X-ray absorption spectroscopy

Malte Behrens[a], Jan Tomforde[a], Enno May[a], Ragnar Kiebach[a], Wolfgang Bensch[a,*], Dietrich Häußler[b], Wolfgang Jäger[b]

[a]Institute of Inorganic Chemistry, Christian-Albrechts-University of Kiel, Olshausenstr. 40-60, 24098 Kiel, Germany
[b]Mikrostrukturanalytik, Technische Fakultät, Christian-Albrechts-University of Kiel, Kaiserstr. 2, 24143 Kiel, Germany

Received 9 March 2006; received in revised form 13 June 2006; accepted 26 June 2006
Available online 29 June 2006

Abstract

The reactivity of [Cr/Se/Te] multilayers under annealing was investigated using X-ray reflectometry, in situ X-ray diffraction, X-ray absorption fine structure (XAFS) measurements and transmission electron microscopy. For all samples, interdiffusion was complete at temperatures between 100 and 300 °C, depending on the repeating tri-layer thickness. A crystalline phase nucleated approximately 20 °C above the temperature where interdiffusion was finished. The first crystalline phase in a binary Cr/Te sample was layered $CrTe_3$ nucleating at 230 °C. In ternary samples (Se:Te = 0.6–1.2), the low-temperature nucleation of such a layered CrQ_3 (Q = Se, Te) phase is suppressed and instead the phase Cr_2Q_3 nucleates first. Interestingly, this phase decomposes around 500 °C into layered CrQ_3. In contrast, binary Cr/Se samples form stable amorphous alloys after interdiffusion and Cr_3Se_4 nucleates around 500 °C as the only crystalline phase. Evaluation of the XAFS data of annealed samples yield Se–Cr distances of 2.568(1) and 2.552(1) Å for Cr_2Q_3 and CrQ_3, respectively. In the latter sample, higher coordination shells around Se are seen accounting for the Se–Te contacts in the structure.
© 2006 Elsevier Inc. All rights reserved.

Keywords: Chromium chalcogenides; Modulated elemental reactants; Multilayer thin films; Anion substitution

1. Introduction

Solid-state syntheses using the so-called modulated elemental reactant (MER) method potentially yield thermodynamically metastable products that often cannot be prepared applying other approaches [1,2]. The alternating deposition of the reactants in form of thin layers yields a multifilm precursor with defined diffusion lengths on the Å-scale [3]. If the repeating unit is sufficiently thin, i.e., below a critical thickness, the interdiffusion of the reactants might be complete at exceptional low temperatures before nucleation of crystalline products occurs. In such systems, the product formation proceeds via an amorphous intermediate [4,5]. For layers thicker than the critical thickness, crystallization is often observed at the interfaces at even lower temperatures. In both cases, the reaction system is usually far from the global minimum of free energy that governs the classical high-temperature methods. Thus, the formation of kinetically stable products is favored by the MER method.

Most exciting new kinetically stable phases were obtained by Johnson and co-workers using the MER method, and fascinating examples are the layered chalcogenide systems $TiSe_2/NbSe_2$ [6,7], $Bi_2Te_3/TiTe_2$ [8] and $VSe_2/TaSe_2$ [9]. Crystalline superlattices like $[(TiSe_2)_n/(NbSe_2)_m]$ composed of a few layers of both binary components were intensively characterized with respect to the synthesis conditions [6,7], lateral structure [10,11], conducting properties [12] and the ability to intercalate transition metal cations in the van der Waals gap [13]. Furthermore, the role of ternary transition metal cations in Mo/Se multilayers has been investigated systematically [14].

*Corresponding author. Fax: +49 4341 880 1520.
E-mail address: wbensch@ac.uni-kiel.de (W. Bensch).

0022-4596/$ - see front matter © 2006 Elsevier Inc. All rights reserved.
doi:10.1016/j.jssc.2006.06.024

Previously, we studied the reactivity of binary Cr/Te [15,16] and Cr/Se multilayers [17]. $[Cr/Se]_m$ samples were found to react via an amorphous alloy that was formed after complete interdiffusion of the elemental layers. From this alloy, highly textured Cr_3Se_4 crystallizes at around 500 °C. For Cr/Te multilayers, the first crystalline phase was observed to be $CrTe_3$. Nucleation occurred at the Cr/Te interfaces at temperatures as low as 100 °C for very thin repeating double-layer thicknesses. In a subsequent step, $CrTe_3$ decomposes into Cr_2Te_3. In conclusion, it can be seen from our previous work that the reactivity of the binary systems is very different and the question concerning the reactivity of mixed systems arises.

Chromium chalcogenides are magnetic and electrical "chameleons": the sulfides show antiferromagnetic properties and semi-conducting behavior; Cr selenides also exhibit antiferromagnetic properties but are better electrical conductors, and finally all tellurides are ferromagnetic and metals. In several contributions, we demonstrated that the magnetic behavior can be altered by adjusting the Cr:Q ratio, or by substituting Te partially by Se leading to complex and fascinating magnetic properties [18–23]. All these experiments were performed on samples prepared at elevated temperatures. Some Cr chalcogenides are candidates for half-metallic ferromagnets that are needed for future applications in spintronic devices [24]. The handling of the ferromagnetic materials in form of thin films is a prerequisite for the production of spintronic elements. Therefore, fundamental investigations are necessary to explore the structures formed in a thin film couple and their thermal stability. In the present paper, we report the effect of anion substitution on the reactivity of thin Cr/Se/Te multilayers.

2. Experimental section

The multilayer films were prepared in an ultra-high-vacuum deposition chamber ($P<10^{-8}$ mbar), which is described in detail elsewhere [25]. Cr/Se/Te tri-layers were deposited on approximately 1 cm^2 (100)-Si single-crystal substrates. Including the substrate, the samples can be described as [Si/native $SiO_x/(Cr/Se/Te)_m$] ($m = 20$, 40 or 50). Chromium (Chempur, 99.99%) was deposited with a Focus EFM 3 electron beam gun with a constant ion flux of 1 μA. Se and Te were evaporated from Knudsen cells controlled by an Oxford Instruments temperature controller at 240 and 400 °C, respectively (Se: Riedel-de Haen, 99.9%; Te: Retorte; 99.999%). The single-layer thicknesses were controlled by variation of the shutter opening times of the evaporation cells. A quartz microbalance (Tectra) was used for calibration. The substrate was kept at ambient temperatures in all experiments.

X-ray data were collected on a Bruker-AXS D8 Advance θ–θ diffractometer (Cu $K\alpha$ radiation) equipped with a Göbel mirror and a Material Research Instruments Reflectometry high-temperature chamber (MRI-HTC). The in situ experiments were performed under high vacuum ($P<10^{-5}$ mbar). The temperature was gradually increased in steps of 10 °C with a heating rate of 0.05 °C/sec and held constant during the collection of X-ray diffraction (XRD) patterns. X-ray reflectometry (XRR) curves were recorded on the same machine in air.

The compositions of the films were determined in a Philips scanning electron microscope (SEM) XL 30 ESEM equipped with an energy dispersive analysis of X-rays (EDAX) system. Due to the small amount of material and the strong substrate peak, an accuracy of about 5 at% was reached.

X-ray absorption fine structure (XAFS) spectra of selected Cr/Se/Te films were collected at the Se *K*-edge with synchrotron radiation at room temperature at the X1 beamline of HASYLAB, Hamburg/GER, using the Si-(111) monochromator. Spectra of the thin films were recorded in the fluorescence mode using a Ge detector. X-ray absorption near edge structure (XANES) and extended X-ray absorption fine structure (EXAFS) were analyzed using the software FEFF [26] and WinXAS [27]. Structural data were elucidated from the spectra by fitting theoretical spectra to the experimental data. The models for the coordination cluster around the absorbing atom base on bulk crystal structures. To reduce the number of free running parameters for the refinements, the coordination numbers were fixed to the values observed in the single-crystal structures.

For transmission electron microscopy (TEM) investigations, the Si substrate was removed from the backside of the sample by subsequent grinding, dimpling and ion bombardment to prepare a free standing film segment. TEM micrographs and electron diffraction patterns were recorded on a Philips CM30 STEM at 300 kV.

3. Results and discussion

The results presented here are a representative selection of the experiments performed and cover seven Cr/Se/Te multilayers with Cr contents ranging from 33 to 58 at%. Two of the samples are binary Cr/Se and Cr/Te multifilms, respectively (CS-21, CT-1). Two have a Se to Te ratio near one (CTS-04, CTS-11), two exhibit a lower ratio near 2/3 (CTS-07, CTS-23) and one film contains only a small amount of Se (CTS-17). The compositions of the samples and the thickness data are summarized in Table 1.

The repeating layer thicknesses were determined from XRR measurements by evaluation of the position of the multilayer modulation peaks caused by the periodic arrangement of the samples (Table 1) [28]. A representative XRR curve (sample CTS-11) is shown in Fig. 1. In the as-deposited state, the XRD patterns of the films showed only a broad modulation together with reflections of the substrate, indicating that the multilayers are in the amorphous state. The reactions of the multifilms under annealing were investigated with in situ XRD. The temperature was increased gradually from room temperature to 600 °C and XRD patterns were recorded every

Table 1
Characteristics of the multilayer samples prepared for this study

	Cr (at%)	Se:Te ratio	Cr/Se/Te repeats	Tri-layer thickness
CT-1	48(5)	no Se	20	16(3) Å
CTS-17	33(5)	0.1	40	16(2) Å
CST-07	37(5)	0.6	20	46(4) Å
CTS-23	43(5)	0.7	40	18(2) Å
CTS-11	34(5)	1.0	20	31(5) Å
CTS-04	58(5)	1.2	20	28(3) Å
CS-21	36(5)	no Te	50	37(4) Å

Deviations for the tri-layer thickness are estimated on the basis of the quality of the XRR curve.

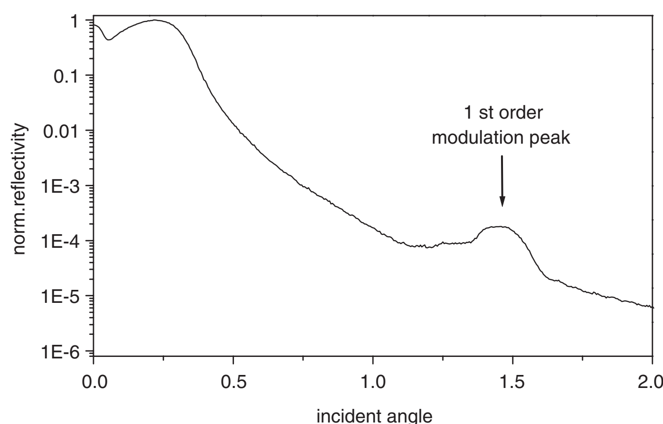

Fig. 1. XRR curve of the sample CTS-11. The maximum is due to the modulated nature of the multilayer and the angular position corresponds to the repeating tri-layer thickness.

10 °C. XRD patterns were also taken during cooling to check the reversibility of the reactions.

First, the results for the binary samples are shortly recalled. The reaction of Cr/Se films has been presented recently [17]. The gradual decay of the modulation peaks indicated that the [Cr/Se] multilayer assembly is destroyed heating to approximately 300 °C. Afterwards, an amorphous Cr–Se alloy exists up to 500 °C and Se is gradually evaporated from the alloy at temperatures above 300 °C. Around 500 °C, Cr_3Se_4 abruptly crystallizes with a preferred (00l) orientation. This reaction pathway, which is represented by Scheme (1), was found to be quite independent of the initial composition and the repeating layer thickness:

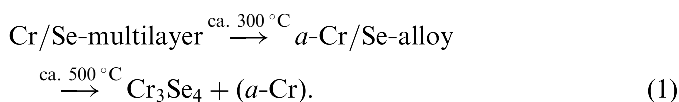

$$\text{Cr/Se-multilayer} \overset{\text{ca. } 300\,^{\circ}\text{C}}{\longrightarrow} a\text{-Cr/Se-alloy} \overset{\text{ca. } 500\,^{\circ}\text{C}}{\longrightarrow} Cr_3Se_4 + (a\text{-Cr}). \quad (1)$$

The binary Cr/Te sample (CT-1) starts to crystallize already at 230 °C as highly textured phase and only one series of reflections can be detected. Nevertheless, an unambiguous identification is possible due to the differences of the Cr_xTe_y structures being derived either from the NiAs type or from the layered CdI_2 type. In both structure types, Cr atom layers reside in the octahedral voids of hexagonally packed Te anions. The positions of reflections of the thin films refer to the layer separation. For Cr_xTe_y compounds exhibiting NiAs-related structures (CrTe, Cr_2Te_3, Cr_3Te_4 and Cr_5Te_8), distances between fully occupied metal atom layers range from 5.731 (Cr_5Te_8 in $F2/m$ [29]) to 6.0895 Å (Cr_3Te_4 in $C2/m$ [30]; for Cr_2Te_3 [31], see Fig. 2). Layered $CrTe_3$ is related to the CdI_2 type [32] and may be considered as metal-deficient $CrTe_2$ and formulated as $Cr_{2/3}Te_2$, although due to Te–Te interactions the hexagonal arrangement of the Te anions is distorted and the layers are slightly wavy. However, the layer separation is significantly larger (6.94 Å, Fig. 2) resulting in X-ray reflections at lower angles (Fig. 3). A good agreement of peak positions and intensities was found for the (h00) and (00l) series of $CrTe_3$ and Cr_2Te_3, respectively.

In accordance with our previously reported results, the first nucleating crystalline phase is (h00) textured $CrTe_3$. At about 350 °C, $CrTe_3$ decomposes into Cr_2Te_3 [15,16] (Fig. 4). This reaction step is assumed to be introduced by the loss of Te. This hypothesis is consistent with a result obtained recently for Cr–Te thin film samples that were covered with a thick Cr capping layer. Evaporation is hampered in such samples and the decomposition of $CrTe_3$ into Cr_2Te_3 does not occur. $CrTe_3$ is observed to be the only stable phase in the temperature range from 300–500 °C in these samples.

The upper temperature limit of the experiments discussed in earlier papers was 500 °C, which is now extended to 600 °C. Interestingly, a further reaction occurs for $T > 470$ °C. The intensity of reflections of Cr_2Te_3 decreases and surprisingly, reflections of $CrTe_3$ start to grow on the cost of Cr_2Te_3 (Fig. 4). The decomposition of bulk Cr_2Te_3 is predicted by the binary equilibrium phase diagram [33] at 455 °C which is in good agreement with the temperature obtained for the thin film sample. According to the phase diagram, the low-T and high-T modifications of $Cr_{3\pm x}Te_4$, respectively, are expected to be the products of this peritectoid reaction. The observation that distinct phases do not occur in thin film reactions although they are favored by composition and/or thermodynamics is not unique [15,17,34,35]. Nucleation barriers are assumed to play a key role in this course. Most interestingly, the crystalline product obtained here is again $CrTe_3$. The growth of the $CrTe_3$ reflections starts at 540 °C at a significantly higher temperature than the onset of the decay of the Cr_2Te_3 reflections. Most likely, the reaction proceeds via an amorphous intermediate. Which phase crystallizes from this intermediate is determined by nucleation barriers. Obviously, $CrTe_3$ is the most favorable phase, again. The crystallization of $Cr_{3\pm x}Te_4$, which is expected from the phase diagram, is probably associated with a very unfavorable nucleation barrier. Consequently, Cr_3Te_4 has never been observed to crystallize as a thin film in our laboratory independent of composition, layer thickness or reaction temperature of binary Cr–Te samples. The decomposition reaction is not complete after annealing to

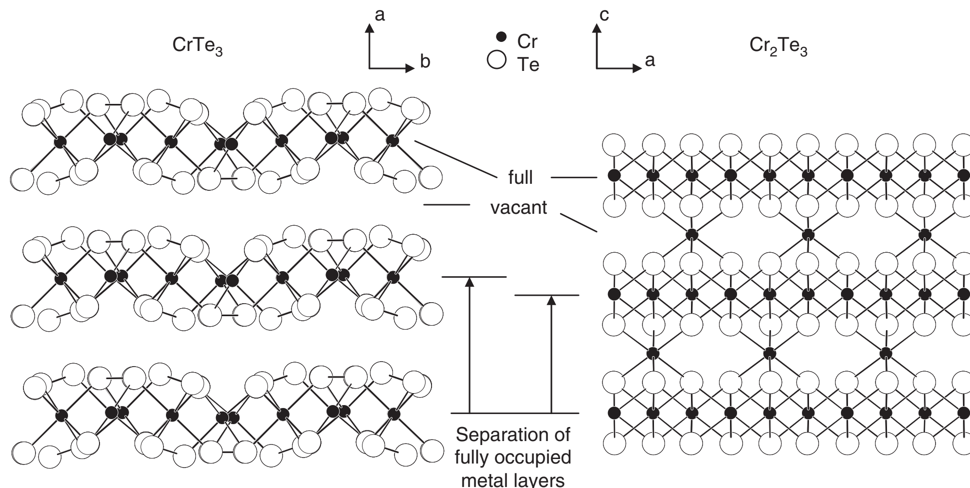

Fig. 2. Crystal structures of $CrTe_3$ (right, view along the *c*-axis) and Cr_2Te_3 (left, view along the *a*-axis) consisting of alternating fully occupied and partially occupied or vacant Cr layers. The difference in layer spacing between two fully occupied Cr layers is marked.

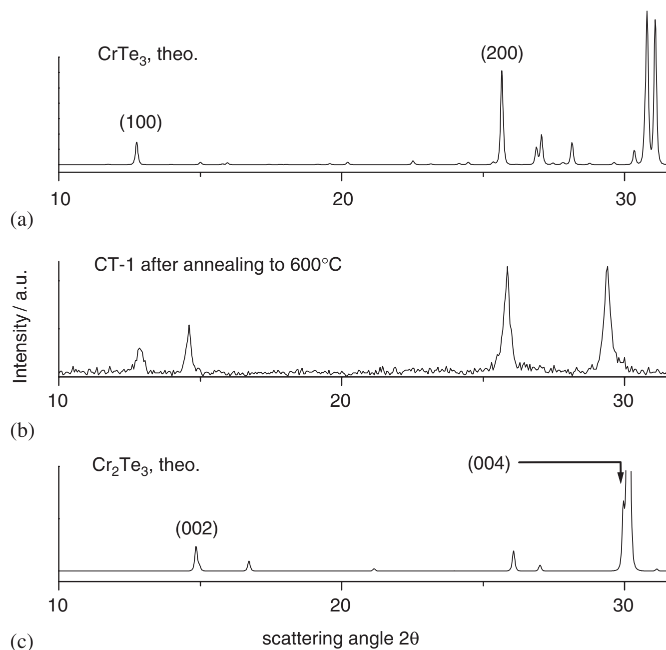

Fig. 3. Theoretical powder patterns of $CrTe_3$ (a), Cr_2Te_3 (c) and of the sample CT-1 after annealing to 600 °C (b) showing that both phases are present.

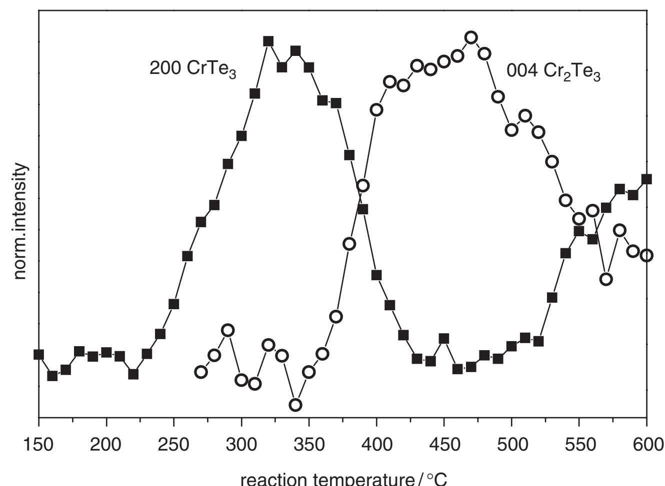

Fig. 4. Normalized integral intensity data for the (200) reflection of $CrTe_3$ and the (004) reflection of Cr_2Te_3 as a function of temperature. The lines are guide for the eyes.

600 °C and both phases are present in the sample CT-1 after annealing (Fig. 3b).

It must be assumed that during the reaction, amorphous Cr is formed. It is known that annealing in dynamical vacuum leads to an evaporation of the chalcogen at high temperatures and the remaining excess of Cr is in the amorphous state [15,17]. The reaction for the film can be represented by Scheme (2):

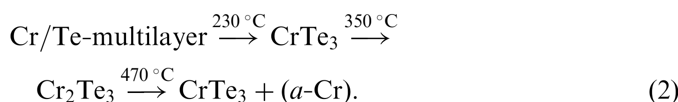

$$\text{Cr/Te-multilayer} \xrightarrow{230\,^{\circ}\text{C}} CrTe_3 \xrightarrow{350\,^{\circ}\text{C}} Cr_2Te_3 \xrightarrow{470\,^{\circ}\text{C}} CrTe_3 + (a\text{-Cr}). \quad (2)$$

Substituting a small amount of Te by Se has minor influences on the reactivity of the multilayer. The in situ XRD patterns of the sample CTS-17 (5 at% Se) are shown in Fig. 5. The modulation peak has vanished at 170 °C, i.e., before nucleation of the crystalline phase. Hence, nucleation does not occur at the interfaces between single layers, but from an amorphous alloy with composition $Cr_{33}Te_{62}Se_5$. The crystallization of the layered CdI_2 derivative $CrTe_{3-x}Se_x$ ($x \approx 0.2$) starts at 210 °C and the decomposition of this phase into $Cr_2Te_{3-x}Se_x$ ($x \approx 0.2$) occurs at 350 °C. An interesting observation is that weak and broad reflections of the NiAs type phase are detected already in the as-deposited multilayer, but pronounced growth does not start below the decomposition temperature of $CrTe_{2.8}Se_{0.2}$. The third step of the reaction occurs at 500 °C, where the intensity of the reflections of the NiAs-related phase decays and the layered phase starts to grow

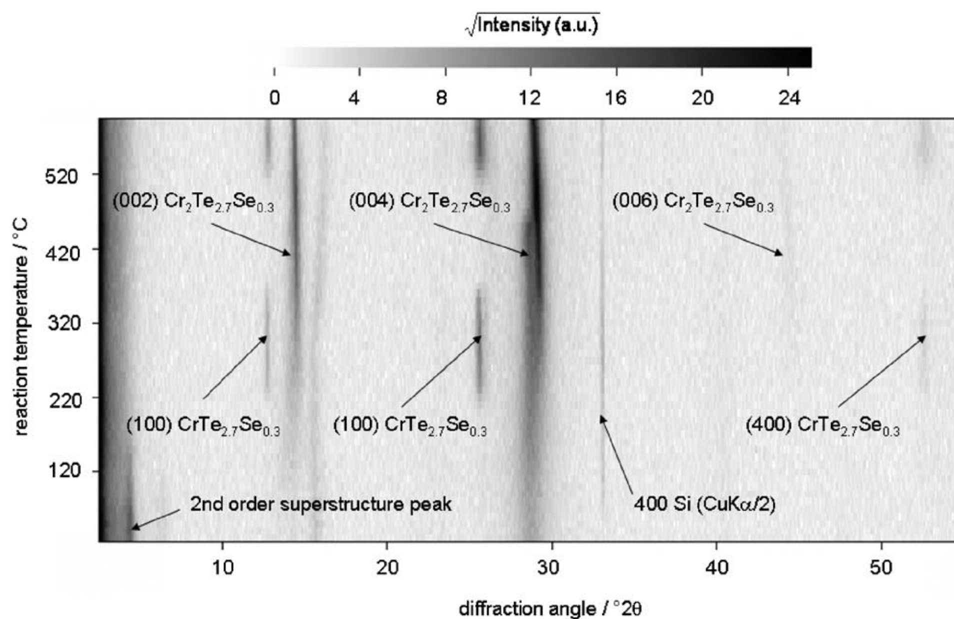

Fig. 5. Evolution of the X-ray intensities of sample CTS-17 collected in situ (top view). Substrate and modulation peaks are marked.

again. Although the transition temperatures slightly differ from the binary sample, it can be concluded that the reactivity of Se-poor ternary multilayers is similar to the Cr/Te system.

The steady shift of the reflections to lower angles (Fig. 5) at high temperatures is due to thermal expansion. The reflections of the high temperature phase $CrTe_{2.8}Se_{0.2}$ were found to shift back during cooling of the film. Apart from these shifts of the peak positions, no other alterations were seen in the patterns during cooling, i.e., the structural changes are irreversible.

For the samples with a higher Se content, a different reaction is observed, but all these films exhibit a similar behavior. Intensity data of the modulation peaks and selected Bragg intensities of the first nucleating phase are shown in Fig. 6 for samples CTS-07 and CTS-23. A pronounced growth of Bragg reflections starts only after the complete decay of the modulated structure. Hence, the ternary multilayer first interdiffuses completely before a crystalline phase nucleates. The complete destruction of the multilayer assembly occurs at 120 °C for CTS-23 (18 Å thick tri-layer) and at 290 °C for CTS-07 (46 Å thick tri-layer).

The high-angle, high-temperature intensity data of the in situ XRD experiments performed on samples CTS-04 and CTS-07 are shown in Fig. 7. The first crystalline phase is $Cr_2Te_{3-x}Se_x$ with a NiAs-type structure occurring at about 300 °C. This observation implies that the nucleation of layered $CrTe_{3-x}Se_x$ is suppressed at low temperatures. Johnson and co-workers observed that the presence of a ternary element ($M =$ Cu, Sn, In) above a critical concentration in the multilayer system M/Mo/Se inhibits the nucleation of $MoSe_2$ at the interfaces which is normally observed in binary samples [14]. Additionally, Johnson et al. discussed the theoretical approach of Desré [36], which

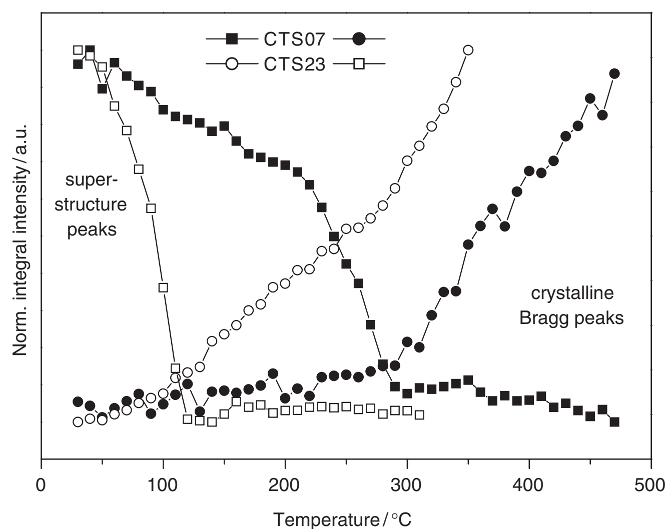

Fig. 6. Low- and high-angle in situ XRD intensity data of the interdiffusion process of the samples CTS-07 and CTS-23. The normalized integral intensity of the modulation peaks and of characteristic Bragg reflections of $Cr_2Te_{3-x}Se_x$ are shown.

predicts a decrease of the probability of a nucleant fluctuation by the factor of 10 for each additional component in a reaction system.

The decomposition of $Cr_2Te_{3-x}Se_x$ into $CrTe_{3-x}Se_x$ starts at 500 °C, as in all other samples (Fig. 7). At 600 °C, the growth of $CrTe_{3-x}Se_x$ is finished for CTS-04, whereas it is not complete for CTS-07. Additionally, the crystallization of fcc-Cr is observed at high temperatures for the Cr-rich sample CTS-04, and obviously the crystalline Cr domains developed during the decomposition of Cr_2Q_3 into CrQ_3 and are large enough to be detected with XRD.

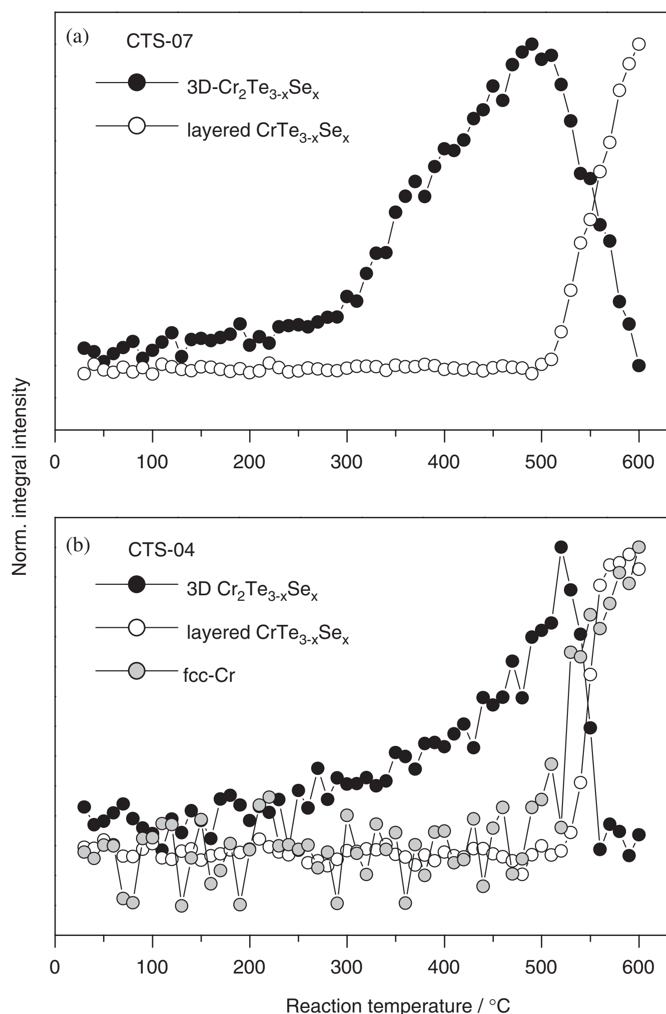

Fig. 7. Normalized integral intensity data for the (004) reflection of $Cr_2Te_{3-x}Se_x$ and the (200) reflection of $CrTe_{3-x}Se_x$ for the samples CTS-07 (a) and CTS-04 (b). Intensity data of the (111) reflection of fcc-Cr are also given in (b). The lines are guides for the eyes.

As in the binary sample CT-1, in the Cr-poorer ternary samples, only very weak modulations could be found instead of sharp reflections for the Cr excess indicating that Cr is amorphous or the domains are very small. It is noted that the crystallization of Cr starts at a temperature 10–20 °C lower than the crystallization of CrQ_3 suggesting again that the nucleation of the latter proceeds via an amorphous intermediate.

A change of composition was detected for all samples after annealing due to evaporation of chalcogen leading to Cr-richer compositions. For example, the initial Cr content for CTS-04 of 58(5)% increased to 78(5)% after heating to 600 °C. We assume that grains of crystalline chalcogenide material are present in a matrix of Cr, which is amorphous in most samples. Accordingly, the chalcogen is enriched in the crystalline chalcogenide grains. While the Cr:Q ratio increased after the heat treatment, the Se:Te ratio remains constant within the limits of accuracy.

The distance between fully occupied metal atom layers of the crystalline phases are elucidated from the positions of the X-ray reflections. For $Cr_2Te_{3-x}Se_x$, the value is 6.06 Å for CT-1 ($x = 0$) and the Se-poor sample CTS-17 ($x = 0.2$), whereas for $x = 1.1$ (CTS-07) the distance is 6.04 Å. In the polycrystalline Cr_3Se_4 film obtained from Cr/Se multilayers, the separation amounts to 5.91 Å [17]. Hence, substitution of Te by the smaller Se leads to a contraction of the unit cell volume. In Cr_5SeTe_7 [18] and $CrSe_{0.4}Te_{0.6}$ [37] bulk samples, Se and Te are distributed statistically over the crystallographically unique sites which can also be assumed for the thin film materials. The layer separations for the layered phase $CrTe_{3-x}Se_x$ do not follow this trend and measure 6.89 Å for all samples.

The local environments around Se atoms in the two crystalline phases were investigated using XAFS spectroscopy (XANES and EXAFS). Se K-edge spectra of the sample CTS-04 after annealing to 600 °C (layered $CrTe_{1.5}Se_{1.5}$) and of sample CTS-11 after annealing to 400 °C ($Cr_2Te_{1.4}Se_{1.6}$) were recorded. The XANES, EXAFS and FT-EXAFS are shown together with XRD results in Fig. 8. A "fingerprint matching" of the two XANES spectra reveals some differences which can be attributed to the different coordination numbers of the chalcogen atoms and to the different electronic situation in both phases. The FT-EXAFS spectra (Fig. 8d) suggest a similar Se–Cr distance for the first coordination shell in both phases. Structural data were elucidated from the spectra by fitting a model cluster developed with crystallographic data [31,32] to the experimental data. The results are summarized in Table 2. For the first Se–Cr shell, distances of 2.568(1) and 2.552(1) Å were obtained for Cr_2Q_3 and CrQ_3, respectively. This minor difference is in agreement with single-crystal data. Chromium is trivalent

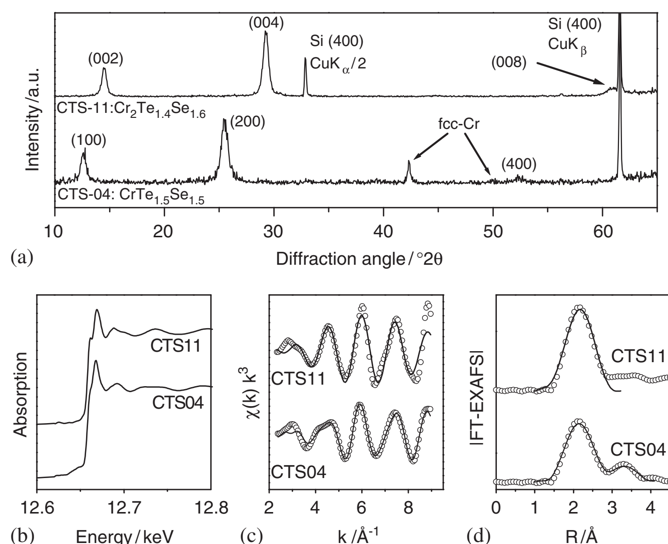

Fig. 8. XRD patterns (a), Se K-XANES spectra (b), $\chi(k)$ EXAFS oscillations (k^3-weighted) (c), and FT-EXAFS magnitude (no correction for EXAFS phase shift) (d) of the samples CTS-11 and CTS-04 after annealing to 400 and 600 °C, respectively. The data for CTS-11 is shifted by an arbitrary amount for clarity in all figures. The points in (c) and (d) represent the experimental data and the lines are the fits.

Table 2
Results of the Se K-edge EXAFS refinements of the samples CTS-04 and CTS-11[a]

	CTS-11 ($Cr_2Te_{1.4}Se_{1.6}$)	CTS-04 ($CrTe_{1.5}Se_{1.5}$)		
Shell	Se–Cr	Se–Cr	Se–Te	Se–Te
CN	4[b]	2[b]	1[b]	2[b]
Distance (Å)	2.568(1)	2.552(1)	3.007(3)	3.471(6)
D–W factor (Å^2)	0.0113(1)	0.0066(1)	0.0141(2)[c]	0.0142(1)[c]
E_0 shift (eV)	10.8(1)	7.2(1)	13.2(4)[d]	13.2(4)[d]

[a] S_0^2 was fixed to 0.9 for all refinements.
[b] Coordination numbers were fixed during refinement.
[c] Parameters correlated using the correlated Debye model.
[d] Parameters correlated to be equal.

in $CrTe_3$ and charge compensation occurs via Te–Te bonding interactions [38]. In an ionic picture, $CrTe_3$ can be formulated as $[(Cr^{3+})_2(Te)^{2-}(Te_2)^{2-}(Te_3)^{2-}]$. On average, it exhibits one short Q–Q and two longer Q–Q bonds for each chalcogen atom. Consequently, higher coordination shells are observed for the samples CTS-04 (Fig. 8d). Assuming Se–Te contacts, average distances of 3.007(3) and 3.471(6) Å are obtained for these higher shells. We note that the first Se–Te shell is not resolved in the FT-EXAFS, but its signal merges with the strong Se–Cr peak. The existence of such a Se–Te shell is suggested by the crystal structure of $CrTe_3$ and supported by the reasonable results of the refinement using this model (Table 2). No such pronounced higher coordination shells are observed for the sample CTS-11 because no Q–Q interactions are present in Cr_2Q_3. It is noted that in the crystal structure, slightly different inter-atomic distances exist within each shell. In the structural model for the fitting procedure, only one Se–Cr distance was considered to keep the number of freely varying parameters small and the values obtained represent average distances. The Debye–Waller factors (D–W factors) contain a contribution of static disorder explaining the relatively low value for the Se–Cr shell in CrQ_3, where only minor differences between the single Se–Cr distances exist.

The metastable Cr_2Q_3 phase of sample CTS-11 was further characterized with electron diffraction. The TEM micrograph and the corresponding electron diffraction pattern are shown in Fig. 9. In the micrograph, three different degrees of shading can be observed. The brightest domains correspond to residuals of the Si wafer and exhibit brush marks originating from the sample preparation process. The darkest domains probe areas of high electron density and should therefore correspond to the chromium chalcogenide. These domains are crystalline and give rise to the electron diffraction pattern in Fig. 9 (upper left corner) and the XRD pattern shown in Fig. 8a, upper curve. Single diffraction spots in the electron diffraction pattern are due to residuals of the Si substrate. The strong texture of the polycrystalline material is manifested by the severe fragmentation of the diffraction rings. A very accurate compositional analysis with EDX was possible for this sample, because the Si substrate was removed during the

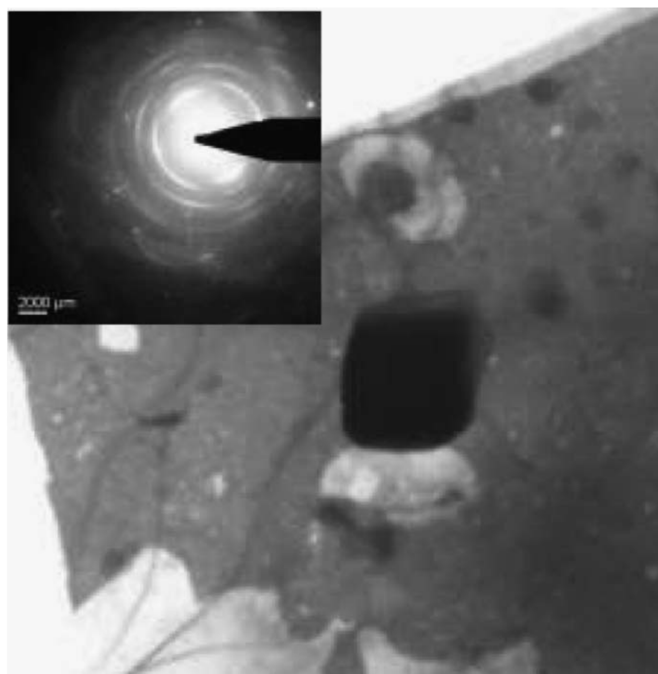

Fig. 9. TEM micrograph and corresponding electron diffraction pattern (upper left corner) of a film segment of the sample CTS-11 after annealing to 400 °C.

TEM sample preparation process and signals of the pure free standing film could be obtained with a high acceleration voltage. Due to evaporation of chalcogen, the Cr content increased significantly from 34(5) to 53.8(2) at% during the annealing process. But the Se:Te ratio was still near 1.2 as in the as-deposited sample. The medium dark areas are assumed to contain the amorphous Cr excess of the sample.

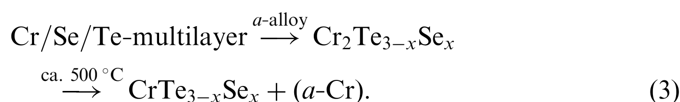

$$\text{Cr/Se/Te-multilayer} \xrightarrow{a\text{-alloy}} Cr_2Te_{3-x}Se_x \xrightarrow{\text{ca. } 500\,^{\circ}\text{C}} CrTe_{3-x}Se_x + (a\text{-Cr}). \quad (3)$$

From these results, the mechanism represented by Scheme (3) can be proposed for the reaction of ternary Cr/Se/Te multilayers with Se:Te ratios between 0.6 and 1.2. In this reaction, the temperature of the first step is determined by the thickness of the repeating tri-layer.

The initial Se:Te is maintained during annealing despite the loss of chalcogen during the heating procedure. For the Cr-richest sample, a fraction of the chromium content is found to be crystalline after the second reaction step.

4. Conclusion

The anion substitution in chromium chalcogenide multilayers has a significant influence on the reactivity of the multifilms. For binary Cr/Se samples, complete interdiffusion and only one crystalline phase, i.e., Cr_3Se_4, were observed in the temperature interval up to 600 °C (Scheme 1). For binary Cr/Te samples, nucleation of layered $CrTe_3$ starts at the interfaces of the elemental layers. The interface-$CrTe_3$ decomposes into Cr_2Te_3, which re-transforms into $CrTe_3$ at higher temperatures (Scheme 2). Se-poor ternary samples react in a similar way. Ternary multilayers (Se:Te = 0.6–1.2) show an intermediate behavior. The material interdiffuses completely and as the first phase $Cr_2Te_{3-x}Se_x$ nucleates from an amorphous alloy, but at significantly lower temperatures than observed for the binary Cr/Se system. Analogous to binary Cr/Te samples, $Cr_2Te_{3-x}Se_x$ decomposes at higher temperatures to form layered $CrTe_{3-x}Se_x$ (Scheme 3).

More work on these complex systems is desirable and clearly needed to understand all these features. The main results of this first study of the effect of substituting Se for Te in chromium chalcogenide multilayers are (a) the "suppression" of the nucleation of a layered phase at low temperatures; (b) the complete interdiffusion before the crystallization of the film or the formation of an interdiffusion intermediate occur; and (c) a trend to smaller layer separations in the NiAs-related phases with increasing Se content.

Acknowledgment

We thank DESY for the allocation of beam-time for the XAFS measurements, Dr. J. Wienold of HASYLAB for her help with the XAFS measurements. We acknowledge the financial support of the State of Schleswig-Holstein and the Deutsche Forschungsgemeinschaft (DFG).

References

[1] M. Noh, C.D. Johnson, M.D. Hornborstel, J. Thiel, D.C. Johnson, Chem. Mater. 8 (1996) 1625.
[2] D.C. Johnson, Curr. Opin. Solid State Mater. Sci. 3 (1988) 159.
[3] L. Fister, D.C. Johnson, J. Am. Chem. Soc. 114 (1992) 4639.
[4] U. Gösele, K.N. Tu, J. Appl. Phys. 66 (1989) 2619.
[5] F. Fukato, M.D. Hornborstel, D.C. Johnson, J. Am. Chem. Soc. 116 (1994) 9136.
[6] M. Noh, J. Thiel, D.C. Johnson, Science 270 (1995) 1181.
[7] M. Noh, D.C. Johnson, Angew. Chem. 108 (1996) 2805.
[8] F.R. Harris, S. Standridge, C. Feik, D.C. Johnson, Angew. Chem. 115 (2003) 5454.
[9] N.T. Nguyen, B. Howe, J.R. Hash, N. Liebrecht, D.C. Johnson, Adv. Mater. 18 (2006) 118.
[10] H.-J. Shin, J. Kwangho, J. Spear, D.C. Johnson, S.D. Kevan, T. Warwick, J. Appl. Phys. 81 (12) (1997) 7787.
[11] H.-J. Shin, K. Jeong, D.C. Johnson, S.D. Kevan, M. Noh, T. Warwick, J. Korean Phys. Soc. 30 (1997) 575.
[12] M. Noh, D.C. Johnson, Chem. Mater. 12 (2000) 2894.
[13] T.A. Hughes, S.D. Kevan, D.E. Cox, D.C. Johnson, J. Am. Chem. Soc. 122 (2000) 8910.
[14] R. Schneidmiller, A. Bentley, M.D. Hornborstel, D.C. Johnson, J. Am. Chem. Soc. 121 (1999) 3142.
[15] S. Kraschinski, S. Herzog, W. Bensch, Solid State Sci. 4 (2002) 1237.
[16] S. Herzog, S. Kraschinski, W. Bensch, Z. Anorg. Allg. Chem. 629 (2003) 1825.
[17] M. Behrens, R. Kiebach, W. Bensch, D. Häußler, W. Jäger, Inorg. Chem. 45 (2006) 2704.
[18] W. Bensch, B. Sander, C. Näther, R.K. Kremer, C. Ritter, Solid State Sci. 3 (2001) 559.
[19] W. Bensch, S. Kraschinski, R.K. Kremer, H. Ebert, Z. Anorg. Allg. Chem. 628 (2002) 2217.
[20] K. Lukoschus, S. Kraschinski, C. Näther, W. Bensch, R.K. Kremer, J. Solid State Chem. 177 (2004) 951.
[21] Z.L. Huang, W. Bensch, D. Benea, H. Ebert, J. Solid State Chem. 177 (2004) 3245.
[22] Z.L. Huang, W. Bensch, D. Benea, H. Ebert, J. Solid State Chem. 178 (2005) 2778.
[23] S. Mankovsky, S. Polesya, H. Ebert, Z.-L. Huang, W. Bensch, Solid State Commun. (2006), in press.
[24] W.-H. Xie, Y.Q. Xu, B.G. Liu, D.G. Pettifor, Phys. Rev. Lett. 91 (2003) 037204.
[25] K. Lokuschus, S. Kraschinski, S. Herzog, W. Bensch, Rev. Sci. Instrum. 72 (2001) 4297.
[26] A.L. Ankudinov, B. Ravel, J.J. Rehr, S.D. Conradson, Phys. Rev. B (1998) 7565.
[27] T. Ressler, WinXAS V3.1, 2004.
[28] V. Holý, U. Pietsch, T. Baumbach, High Resolution X-ray Scattering from Thin Films and Multilayers, Springer, Berlin, 1999, p. 119.
[29] W. Bensch, O. Helmer, C. Näther, Mater. Res. Bull. 32 (1997) 305.
[30] M. Chevreton, E.F. Bertaut, F. Jellinek, Acta Crystallogr. 16 (1963) 431.
[31] A.F. Andresen, Acta Chem. Scand. 24 (1970) 3495.
[32] K.O. Klepp, H. Ipser, Angew. Chem. 94 (1982) 931.
[33] H. Ipser, K.L. Komarek, K.O. Klepp, J. Less-common Met. 92 (1983) 265.
[34] J.M. Jensen, S. Ly, D.C. Johnson, Chem. Mater. 15 (2003) 4200.
[35] M. Overbay, T. Novet, D.C. Johnson, J. Solid State Chem. 123 (1996) 337.
[36] P.J. Desré, J. Mater. Trans. JIM 38 (1997) 583.
[37] I. Tsubokawa, J. Phys. Soc. Japan 11 (1956) 662.
[38] E. Canadell, S. Jobic, R. Brec, J. Rouxel, J. Solid State Chem. 98 (1992) 59.